Entropic stochastic resonance enables trapping under periodic confinement: A Brownian-dynamics study

Nan Shi and Victor M. Ugaz*

Artie McFerrin Department of Chemical Engineering, Texas A&M University, College Station, Texas 77843-3122, USA

(Received 13 October 2013; published 23 January 2014)

Entropically mediated phenomena are of emerging interest as a driving force for microscale and nanoscale transport, but their underlying stochastic nature makes them challenging to rationally manipulate and control. Stochastic resonance offers an intriguing avenue to overcome these difficulties by establishing a clear connection between the system response (the output) and an externally imposed driving force (the input). Previous studies have generally adopted a signal-processing viewpoint to classify the output in terms of a signal-to-noise ratio, but this link does not convey information that is immediately useful to infer parameters relevant to transport. Here we address this issue by applying Brownian-dynamics simulations to elucidate the residence time distribution encountered by a particle as it travels through a channel incorporating periodic constrictions. A sinusoidal longitudinal driving force is applied with a superimposed continuous orthogonal component, making it possible to identify frequency and amplitude conditions where temporal coherence with the particle's motion can be achieved. This resonant state reflects a synergistic combination of geometry and driving force that can be exploited to confine species at discrete locations, offering possibilities for directed manipulation.

DOI: 10.1103/PhysRevE.89.012138 PACS number(s): 05.40.−a

I. INTRODUCTION

Transport of particles and particlelike species in microscale and nanoscale confined environments occurs in a variety of contexts including translocation of small biomolecules through nanopores [1], biological ion channels [2], and DNA separations in nanofilters [3]. These systems impose an energy barrier associated with reduced conformational freedom in a constriction connecting two neighboring larger spaces. Transport under these conditions is characterized by discrete hops across the constricted regions—a process often referred to as entropic trapping. A weak external driving force can alter this free-energy landscape, partially compensating for the entropic penalty. Kramers [4] considered this mode of transport and obtained an expression for the characteristic hopping frequency (escape rate) in terms of the entropic energy barrier, the driving force, and the species' thermal energy. However, the escape rate distribution is inherently broad, reflecting the underlying random thermal motion that enables successful hops to occur.

More recent work has suggested the intriguing possibility that randomness can play a constructive role, enabling the system response to be rationally manipulated by applying a periodic external driving force in a controlled manner [5]. In this way, it is possible to achieve synchronization between the hopping events and the driving force, a condition known as stochastic resonance (SR). In pioneering work [6–8], Hänggi and co-workers demonstrated that SR could be achieved in entropy-dominated particle transport actuated by a periodic driving force with a superimposed continuous orthogonal component, yielding enhanced spectral amplification. Unfortunately, the signal-processing viewpoint traditionally used to describe these resonant effects (e.g., in terms of maximizing the signal-to-noise ratio) does not convey information immediately useful to connect resonance with transport parameters relevant to particle manipulation. From the experimental side, Spagnolo and co-workers demonstrated the emergence of stochastic resonance behavior in a bistable electronic device, i.e., the tunnel diode, and also the dynamics of short polymer translocation driven by an oscillating force [9–11]. These studies revealed many intriguing phenomena such as resonant crossing of the energy barrier and enhanced diffusion by manipulation of the system noise strength [12–14]. Here we focus on the residence time distribution of Brownian species in a spatially periodic array of constrictions under the influence of a temporally periodic longitudinal driving force with a constant transverse component [6–8] and employ Brownian-dynamics simulations to elucidate how proper selection of parameters associated with both domains of periodicity makes it possible to induce resonance associated with the escape rate from the local energy barrier. A key difference between our approach and those in the aforementioned references is that we achieve SR by tuning the frequency and amplitude of an external periodic force, in contrast to previous studies where SR effects were accessed by tuning the noise strength. Our formulation makes it possible to design systems of particular relevance to biological and separation applications where the underlying randomness associated with entropic phenomena can be exploited to direct species transport in a controlled way.

II. RESULTS AND DISCUSSION

A. Stochastic resonance in a single constriction geometry

We begin by considering a two-dimensional topology consisting of upper and lower bounding surfaces that impose periodically spaced constrictions [Fig. 1(a)]. The resulting cross-sectional profile is defined as [7]

$$w_{\pm} = \mp L_y\left(\frac{x}{L_x}\right)^4 \pm 2L_y\left(\frac{x}{L_x}\right)^2 \pm \frac{b}{2}L_x, \qquad (1)$$

*Author to whom correspondence should be addressed: ugaz@tamu.edu

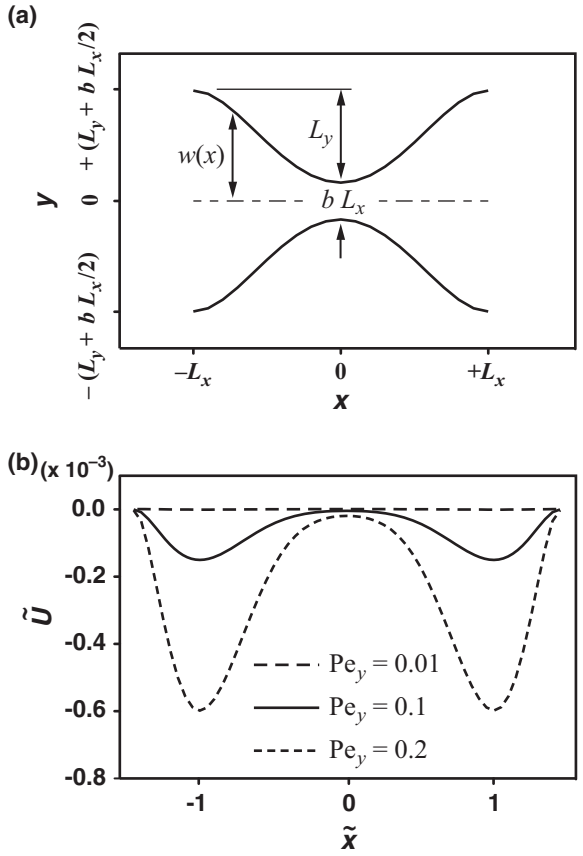

FIG. 1. Confinement geometry and energy landscape. (a) The microchannel geometry considered incorporates periodically spaced constrictions $w(x)$ described by Eq. (1). In terms of scaled variables, the narrowest and widest regions are defined by b and $2\varepsilon + b$, respectively (in this study we choose $b = 0.1$ and $\varepsilon = 0.25$). A time-periodic driving force F_x is applied along the x direction and a constant transverse force F_y is imposed in the y direction. (b) The scaled energy landscape in the absence of the driving force F_x is approximated by a double potential well, where the energy maxima and minima are located at $\tilde{x}_{\max} = 0$ and $\tilde{x}_{\pm\min} = \pm 1$, respectively. Energy landscapes are plotted for three different scaled transverse force conditions expressed in terms of Pe_y. The energy barrier vanishes when the magnitude of the transverse force is small ($Pe_y = 0.01$ and $\tilde{U} \approx 0$), becoming steeper and eventually losing the entropic contribution as the transverse force increases [8]. We assume $Pe_y = 0.1$ in the subsequent analysis.

where the upper and lower walls of the channel are denoted by w_+ and w_-, respectively. The constriction width at $x = 0$ is defined by the product $L_x b$, where L_x is the axial distance from the constriction to the maximum channel width position ($x = L_x$ or $-L_x$). The product $2L_y$ expresses the reduction in channel width from $x = L_x$ or $-L_x$ to the constriction at $x = 0$.

Transport is formulated in terms of the Langevin equation describing overdamped particle motion

$$\gamma \frac{d\mathbf{r}}{dt} = -G\mathbf{e_y} + F(t)\mathbf{e_x} + \mathbf{F_B}, \tag{2}$$

where $\mathbf{F_B}$ is the Brownian force with zero mean and correlation function $\langle \mathbf{F_B}(t)\mathbf{F_B}(t')\rangle = 2k_BT\gamma\delta(t-t')$, k_B is Boltzmann's constant, T is absolute temperature, γ is the friction coefficient, $\mathbf{r}$ represents the position of the particle (Cartesian coordinates with unit vectors $\mathbf{e_x}$ and $\mathbf{e_y}$ in the x and y directions, respectively), G is the magnitude of the transverse force, and the longitudinal sinusoidal force has the form $F(t) = F_0 \sin(\Omega t)$.

Equations (1) and (2) are made dimensionless using a base length scale L_x, time scale $\gamma L_x^2/k_BT$, and force k_BT/L_x, yielding

$$\tilde{w}_\pm = \mp\varepsilon\tilde{x}^4 \pm 2\varepsilon\tilde{x}^2 \pm \frac{b}{2}, \tag{3}$$

$$\frac{d\tilde{\mathbf{r}}}{d\tilde{t}} = -\mathrm{Pe}_y\mathbf{e_y} + \mathrm{Pe}_x(\tilde{t})\mathbf{e_x} + \tilde{\mathbf{F}}_\mathbf{B} \tag{4}$$

in terms of the dimensionless variables $\tilde{w}$, $\tilde{x}$, $\tilde{r}$, and $\tilde{t}$, where $\varepsilon = L_y/L_x$. Two Péclet coefficients are defined as $\mathrm{Pe}_y = GL_x/k_BT$ and $\mathrm{Pe}_x(\tilde{t}) = \tilde{F}_0\sin(\tilde{\Omega}\tilde{t})$, with $\tilde{F}_0 = F_0L_x/k_BT$. Note that γ and F_0 are both species dependent. Following Kim *et al.* [15], we express the Brownian force as $\mathbf{F_B} = (\frac{4\gamma k_BT}{\delta t})^{1/2}\mathbf{n_i}$, where δt is the time step used in the simulation and $\mathbf{n_i}$ is a random vector with each component uniformly distributed over [–1,1]. We then obtain a scaled Brownian force $\tilde{\mathbf{F}}_\mathbf{B} = \sqrt{4/\delta\tilde{t}}\mathbf{n_i}$.

Next we express the energy landscape by assuming a pseudohomogeneous field (i.e., forces do not vary in the y direction). In this way, the y-averaged potential can be used to obtain a simplified expression in the absence of a longitudinal force that depends only on the particle's x position [8]

$$U(x) = -(k_BT)\ln\left(\frac{\int_{w_-}^{w_+} e^{-U(x,y)/k_BT}dy}{w_+ - w_-}\right). \tag{5}$$

Substituting $U(x,y) = Gy$ into Eq. (5) and scaling the energy by k_BT enables the landscape to be expressed by the one-dimensional relationship

$$\tilde{U}(\tilde{x}) = -\ln\left[\frac{1}{(\tilde{w}_+ - \tilde{w}_-)\mathrm{Pe}_y}(e^{-\mathrm{Pe}_y\tilde{w}_-} - e^{-\mathrm{Pe}_y\tilde{w}_+})\right], \tag{6}$$

where the maximum and minimum energies are located at $\tilde{x} = 0$ and ± 1, respectively [Fig. 1(b)]. The trap strength is therefore controlled by the magnitude of G in the unperturbed system.

Now we consider application of a time-periodic longitudinal driving force and ask how its period $\tilde{\Gamma} = 2\pi/\tilde{\Omega}$ can be tuned to match the escape rate from the local energy barrier (i.e., $2\pi/\tilde{\Omega} \sim 1/\tilde{r}_K$, where $\tilde{r}_K$ is the escape rate) [5]. In the absence of the longitudinal force, the scaled escape rate in the energy landscape described by Eq. (5) is given by the Kramers formula

$$\tilde{r}_K = \frac{\sqrt{-\left(\frac{d^2\tilde{U}(\tilde{x})}{d\tilde{x}^2}\big|_{\tilde{x}=0}\right)\left(\frac{d^2\tilde{U}(\tilde{x})}{d\tilde{x}^2}\big|_{\tilde{x}=1}\right)}}{2\pi} \times \exp[\tilde{U}(\tilde{x})|_{\tilde{x}=1} - \tilde{U}(\tilde{x})|_{\tilde{x}=0}]. \tag{7}$$

A trial-and-error approach is sufficient to identify a resonance condition associated with parameter values $\mathrm{Pe}_y = 0.1$, $\tilde{\Omega} = 0.01$, and $\tilde{F}_0 = 0.05$. Since the system state at SR is sensitively impacted by these values [Fig. 2(a)], this method is

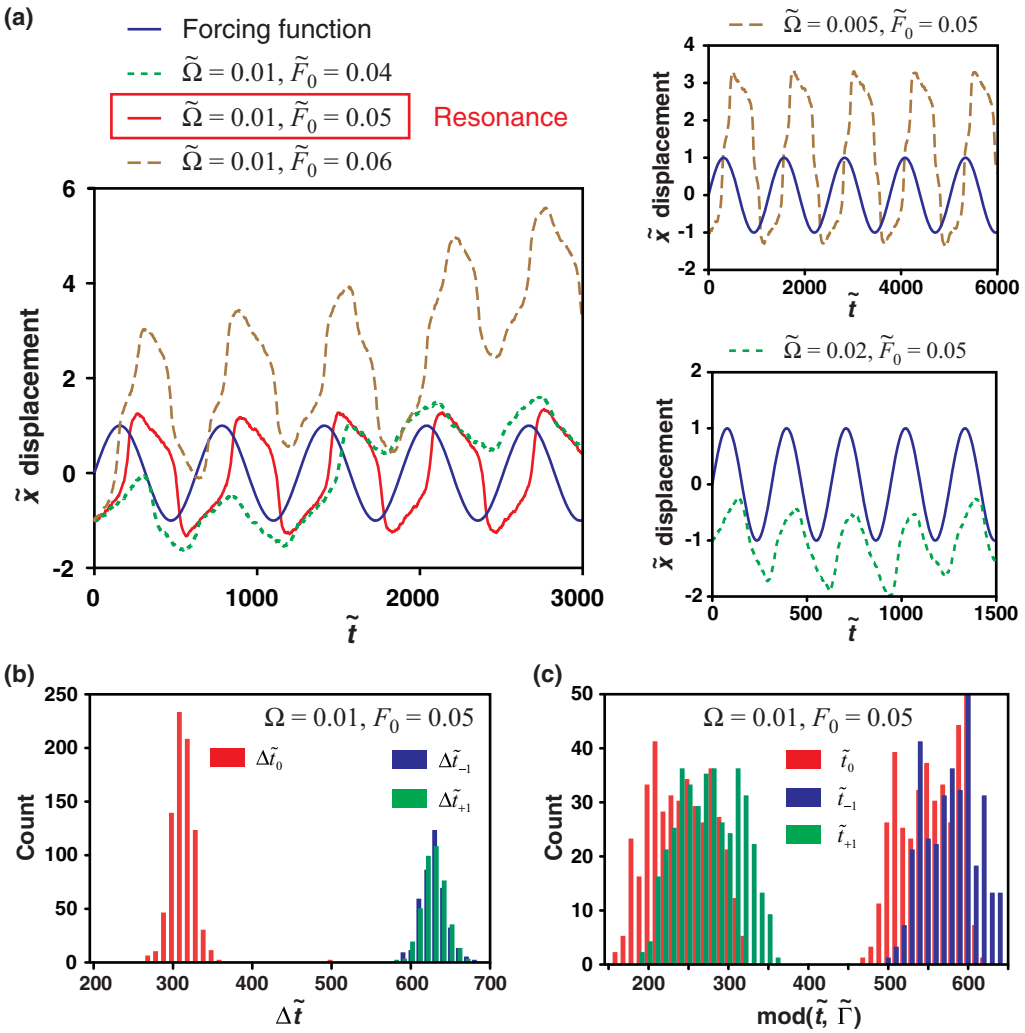

FIG. 2. (Color online) Stochastic resonance in the confining geometry. (a) Stochastic resonance occurs in the confining microchannel depicted in Fig. 1(a) when $\tilde{F}_0 = 0.05$, $\tilde{\Omega} = 0.01$, and $\mathrm{Pe}_y = 0.1$. Transport of Brownian particles in response to a periodic driving force (period $\tilde{\Gamma} = 628$, initial location at $\tilde{x} = -1$) causes their position to oscillate between $\tilde{x} = 1$ and -1 at a similar period but with a phase lag. The effects of driving force amplitude $\tilde{F}_0$ and frequency $\tilde{\Omega}$ on particle displacement are shown. (b) Statistical distributions of the time interval between passages through successive energy maxima ($\tilde{x} = 0$) and minima ($\tilde{x} = \pm 1$) display synchronization with the driving force period ($\tilde{\Gamma} = 628$), where $\tilde{t}_0$, $\tilde{t}_1$, and $\tilde{t}_{-1}$ represent the time between successive crossings. The average value of $\tilde{t}_0$ is approximately half of the driving force period due to the fact that each species passes through the energy maximum position twice in a single oscillatory period. (c) After dividing the time intervals in (b) by $\tilde{\Gamma}$, a histogram of the remainder is plotted to reveal the corresponding phase lag distributions. A comparison of the averages associated with $\tilde{t}_{-1}$ and $\tilde{t}_1$ to $3\tilde{\Gamma}/4 = 471$ and $\tilde{\Gamma}/4 = 157$ yields a characteristic phase lag of $\tilde{t}_{\mathrm{lag}} \approx 100$.

appropriate for the purposes of our study, where the primary goal is to illustrate the key phenomena. Substituting $\mathrm{Pe}_y = 0.1$ into Eq. (7) yields a characteristic escape rate of $\tilde{r}_K \sim 10^{-4}$ in the unperturbed system. This analysis suggests that an order of magnitude increase in the escape rate is attainable by lowering the energy barrier via the periodically applied driving force $\tilde{r}_K = (\frac{2\pi}{\tilde{\Omega}})^{-1} = 1.6 \times 10^{-3}$. Notice that we ensure that the model is applied only in the entropic regime by imposing a relatively small transverse force Pe_y [8].

B. Stochastic resonance-mediated trapping

A key manifestation of SR is attainment of coherence between a species' oscillatory motion and an imposed periodic driving force, suggesting potential to achieve selective immobilization or separation in an appropriately designed microchannel network. To explore this possibility in the context of the simplified geometry depicted in Fig. 1(a), we employed Brownian-dynamics simulations to monitor particle displacements over a simulation time encompassing 250 driving force periods [Fig. 2(a)]. These data were analyzed to identify times associated with transit through the energy maximum and minimum positions in Fig. 1(b) ($\tilde{t}_{x=0}$ and $\tilde{t}_{x=\pm 1}$, respectively). A histogram of the time intervals between each passage through successive energy maxima and minima ($\Delta\tilde{t}_0$ and $\Delta\tilde{t}_{\pm 1}$, respectively) reveals a narrow distribution centered around a mean value close to the driving force period $\tilde{\Gamma} = 628$ [Fig. 2(b)]. This high degree of synchronization is accompanied by a phase shift between the applied driving force and particle displacement through

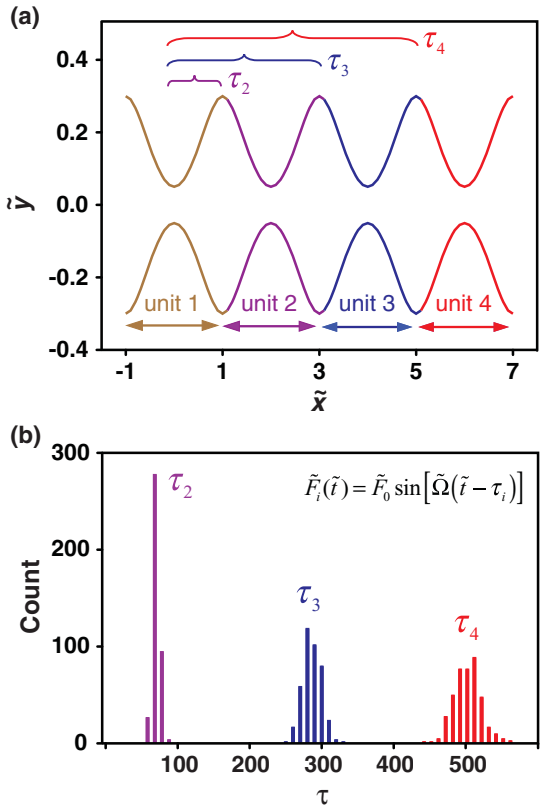

FIG. 3. (Color online) Array of repeated periodic geometries for trapping and separation. (a) A microchannel based on the arrangement depicted in Fig. 1(a) incorporates four repeated constriction units. Energy minima are located at $\tilde{x} = -1$, 1, 3, 5, and 7. Energy maxima are located at $\tilde{x} = 0$, 2, 4, and 6. (b) Phase shifts in the applied driving force τ_i ($i = 2$, 3, and 4) are applied to direct confinement within the corresponding constriction units. The distribution of these phase shifts is obtained from Brownian-dynamics simulation of a 400-particle ensemble, yielding $\langle\tau_2\rangle \approx \langle\tilde{t}_{\tilde{x}=1} - \tilde{t}_{\tilde{x}=0}\rangle \sim 100$ and $\langle\tau_3\rangle - \langle\tau_2\rangle \approx \langle\tau_4\rangle - \langle\tau_3\rangle \approx \langle\tilde{t}_{\tilde{x}=1} - \tilde{t}_{\tilde{x}=-1}\rangle \sim 200$ ($\langle\tau_1\rangle = 0$ by default since particles are initially located at $\tilde{x} = 0$ in unit 1). Resonant conditions of $\tilde{F}_0 = 0.05$, $\tilde{\Omega} = 0.01$, and $\mathrm{Pe}_y = 0.1$ are imposed with particles initially located at $\tilde{x} = 0$.

the microchannel. Closer examination of our data reveals a characteristic phase lag of $\tilde{t}_{\mathrm{lag}} \approx 100$ [Fig. 2(c)], in good agreement with the theoretically predicted value obtained from $\tilde{t}_{\mathrm{lag}}\tilde{\Omega} = \bar{\varphi} \approx \arctan(\tilde{\Omega}/2\tilde{r}_K)$ [16].

C. Trapping in a geometry with repeating constriction units

We next consider a topology containing repeated constriction units bridging adjacent segments of wider cross section [Fig. 3(a)]. Transport between successive constriction units can be achieved by applying a driving force with different phase values in each unit as

$$\tilde{F}_i(\tilde{t}) = \tilde{F}_0 \sin[\tilde{\Omega}(\tilde{t} - \tau_i)], \tag{8}$$

where τ_i ($i = 2$, 3, and 4) compensates for the time associated with each particle's entry into each unit ($\tau_1 = 0$ by default since particles are initially located in unit 1). The average value of τ is determined from the aforementioned synchronization between transport and the applied driving force.

We determined the τ_i values by simulating the displacements of an ensemble of 400 particles through the microchannel geometry shown in Fig. 3(a) and recording the time of initial entry into each subsequent constriction unit. Once a particle in constriction unit i travels beyond the energy minimum in the adjacent zone of larger cross section, the driving force is switched to a value corresponding to unit $i + 1$ with τ_{i+1} [Eq. (8)], while the transverse force is held constant. The resulting distributions [Fig. 3(b)] confirm that transit times are narrowly distributed with average values $\langle\tau_3\rangle = 300$ and $\langle\tau_4\rangle = 500$, consistent with the results in Fig. 2(c). As a result of resonance behavior, the time interval during which species travel between $\tilde{x}_{\max}$ and $\tilde{x}_{\pm\min}$ in each constriction unit [e.g., $\tilde{x} = 0$ and $\tilde{x} = \pm 1$ in Fig. 1(b)] is narrowly distributed. In this framework, τ_2 represents the time to travel from $\tilde{x}_{\max}$ to $\tilde{x}_{\min}$ within the first unit [i.e., corresponding to $\langle\tilde{t}_{\tilde{x}=1} - \tilde{t}_{\tilde{x}=0}\rangle \sim 100$ in Fig. 3(b)], whereas the subsequent τ_i correspond to the transit times associated with traveling between $\tilde{x}_{\pm\min}$ in successive units [i.e., $\langle\tilde{t}_{\tilde{x}=1} - \tilde{t}_{\tilde{x}=-1}\rangle \sim 200$ in Fig. 3(b)]. By applying these τ_i values, species can be successfully trapped at prescribed locations (Fig. 4).

D. Confinement stability and sensitivity

An important potential application of these resonance phenomena is separation of a target species from different-sized background components. To explore the feasibility of employing SR in this way, we characterized trapping stability and sensitivity to the applied driving force by simulating an ensemble of 400 particles during 100 driving force periods over a range of peak amplitude values $\tilde{F}_0$ in the geometry shown in Fig. 3(a). The influence of $\tilde{F}_0$ on trap stability in the fourth constriction unit is visually depicted by the trajectories in Fig. 5(a). Stable trapping is sustained only at resonance ($\mathrm{Pe}_y = 0.1$, $\tilde{\Omega} = 0.01$, and $\tilde{F}_0 = 0.05$), whereas particles escape the trap and diffuse away with nontrivial probability under other conditions. These trends are clearly seen when displacements are quantified in terms of a survival percentage (i.e., the instantaneous fraction of species that remain trapped [Fig. 5(b)]). The onset of trapping is signaled by an initial jump in survival percentage from zero to unity as $\tilde{F}_0$ approaches the resonant value of 0.05, but the weak confinement gives way to a steady decrease in survival percentage toward zero at a rate dependent on the extent to which $\tilde{F}_0$ deviates from resonance. In contrast, trapping stability dramatically increases once resonance is established, with the survival percentage remaining solidly near unity for over 100 driving force periods. Trapping is extremely selective owing to the sensitive dependence of the resonant state on system parameters (e.g., a 10% decrease in $\tilde{F}_0$ from 0.05 to 0.045 enables escape from the trap after approximately ten driving force periods).

III. CONCLUSION

In this paper, we have explored resonant transport in a microchannel geometry incorporating a spatially periodic array of constrictions under the influence of a temporally periodic driving force. Proper selection of the parameters associated with both domains of periodicity makes it possible

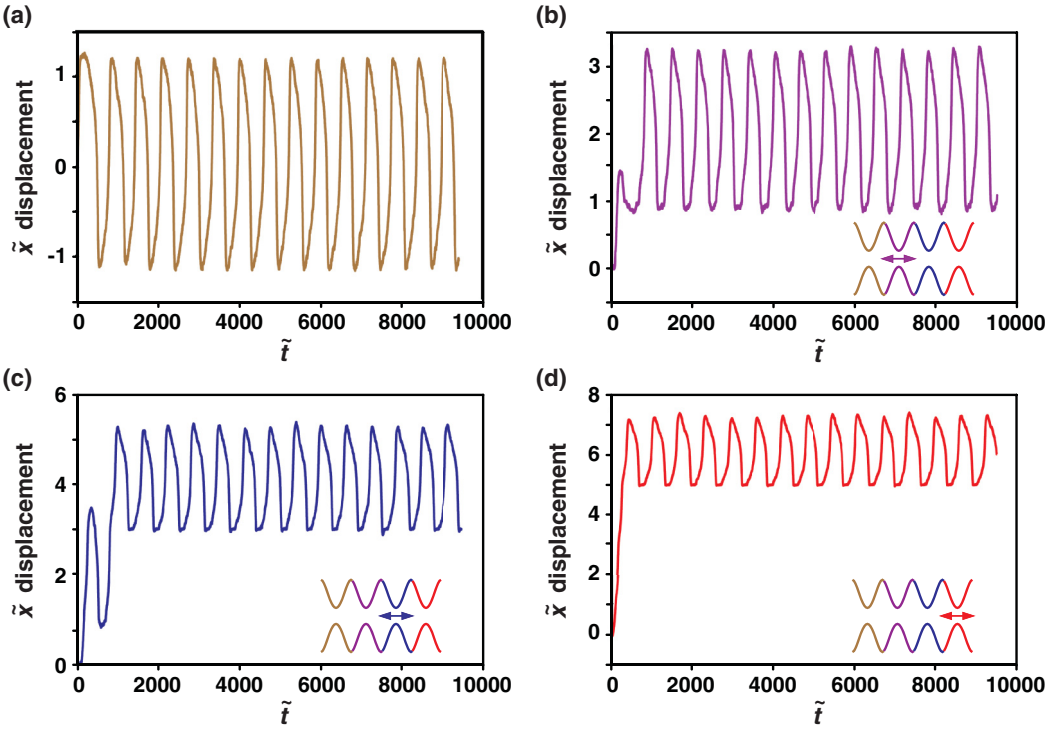

FIG. 4. (Color online) Trapping in a microchannel with periodic confinement. Individual x-displacement trajectories are plotted corresponding to confinement in constriction units (a) 1, (b) 2, (c) 3, and (d) 4 over a time interval of 15 driving force periods (particles are initially located at $\tilde{x} = 0$). The phase value τ_i of the driving force applied in each constriction unit is set to the average values obtained from the distributions in Fig. 3(b) (the transverse force is held constant in all constriction units). In all cases the periodic driving force $\tilde{F}_0 \sin(\tilde{\Omega}\tilde{t})$ is initially applied uniformly throughout the entire geometry. Upon particle entry into an adjacent constriction unit, the periodic force is switched to $\tilde{F}_0 \sin[\tilde{\Omega}(\tilde{t} - \tau_i)]$, while the driving force in the previous constriction unit remains unchanged. Resonant conditions of $\tilde{F}_0 = 0.05$, $\tilde{\Omega} = 0.01$, and $\mathrm{Pe}_y = 0.1$ are imposed, yielding stable confinement in each constriction unit.

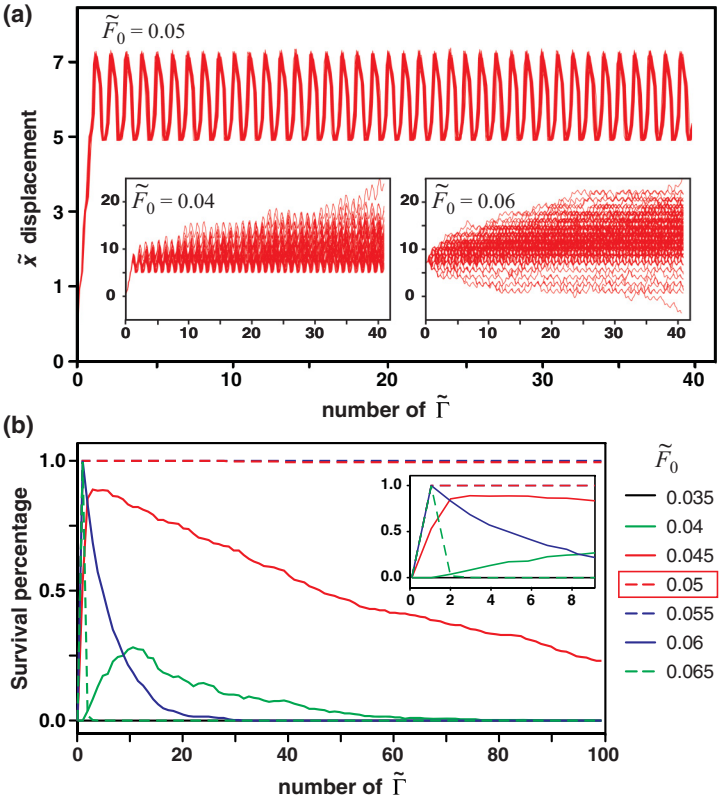

FIG. 5. (Color online) Influence of the periodically applied driving force amplitude on stability and sensitivity of trapping. (a) The x displacement of an ensemble of 400 particles is plotted over 40 oscillatory driving force periods under conditions corresponding to Fig. 4(d). Stable confinement within the fourth constriction region is evident under resonant conditions ($\tilde{F}_0 = 0.05$). Trapping becomes unstable as $\tilde{F}_0$ deviates from resonance, as evident by trajectories that become broadly dispersed away from the trap location. (b) Data tracking the fraction of the 400-particle ensemble that remains trapped between $\tilde{x} = 5$ and 7 over a time scale of 100 driving force periods are plotted for different force amplitudes. Under conditions far away from the resonant value of 0.05 (i.e., $\tilde{F}_0 = 0.06$, 0.045, and 0.04), the survival percentage curves initially increase to 1, but then quickly decay back to 0, indicating very weak confinement. Trapping completely breaks down at $\tilde{F}_0$ values that deviate even farther from resonance, as evident by the survival percentage remaining virtually unchanged from 0 (i.e., $\tilde{F}_0 = 0.065$ and 0.035). Remarkably stable trapping is attained at resonance when $\tilde{F}_0$ is close to 0.05, where the survival percentage reaches and maintains a value of 1 throughout the entire simulation time. Conditions of $\tilde{\Omega} = 0.01$ and $\mathrm{Pe}_y = 0.1$ are imposed in all cases with particles initially located at $\tilde{x} = 0$.

to induce stochastic resonance associated with escape from the local energy barrier. Instead of the concept of signal-to-noise ratio employed in most previous literature involving SR, we have examined the rate of species displacement through the energy landscape and its degree of synchronization with the periodically applied driving force. The period of particle motion and its phase difference with the driving force were quantified by Brownian dynamics simulations, yielding results that display good agreement with the established theoretical understanding of SR. We demonstrated application of this idea in the context of a microchannel geometry incorporating periodic constrictions and modulated the periodic driving force at a different phase in each constriction unit so that particles become selectively confined at prescribed locations within the network.

To obtain a sense of scale for these effects we consider transport of a 50-nm species carrying a charge of $10e$ in the constriction unit geometry of Fig. 1(a), where the microchannel is 3 μm wide at $\tilde{x} = \pm 1$ and 0.5 μm wide at $\tilde{x} = 0$ and $L_x = 5\,\mu$m. A potential on the order of 1 mV would be required to actuate transport between successive energy minima in this configuration, suggesting that a standard AA-size battery could be capable of providing a sufficient driving force to direct transport through an array of 1000 constriction units (on a scale of the order of 1 cm). Stochastic resonance-based approaches also may help overcome limitations of electrostatic-based trapping because low-salt buffering conditions are not required to augment the electrostatic double layer. This level of robustness, combined with the ability to achieve highly stable and selective trapping, suggests the intriguing possibility of exploiting SR effects as an alternative approach to perform manipulation and sorting at the microscale.

ACKNOWLEDGMENTS

V.M.U. gratefully acknowledges support from the US National Science Foundation under Grant No. CBET-1160010, the Camille & Henry Dreyfus Foundation, and the K.R. Hall Professorship at Texas A&M.

[1] Z. D. Harms, K. B. Mogensen, P. S. Nunes, K. Zhou, B. W. Hildenbrand, I. Mitra, Z. Tan, A. Zlotnick, J. P. Kutter, and S. C. Jacobson, Anal. Chem. **83**, 9573 (2011).
[2] C. Y. Lee, W. Choi, J. H. Han, and M. S. Strano, Science **329**, 1320 (2010).
[3] J. Fu, J. Yoo, and J. Han, Phys. Rev. Lett. **97**, 018103 (2006).
[4] H. A. Kramers, Physica **4**, 284 (1940).
[5] L. Gammaitoni, P. Hänggi, P. Jung, and F. Marchesoni, Rev. Mod. Phys. **70**, 223 (1998).
[6] D. Reguera, G. Schmid, P. Burada, J. Rubí, P. Reimann, and P. Hänggi, Phys. Rev. Lett. **96**, 130603 (2006).
[7] P. Burada, G. Schmid, D. Reguera, M. Vainstein, J. Rubi, and P. Hänggi, Phys. Rev. Lett. **101**, 130602 (2008).
[8] P. S. Burada, G. Schmid, D. Reguera, J. M. Rubi, and P. Hänggi, Eur. Phys. J. B **69**, 11 (2009).
[9] E. Lanzara, Am. J. Phys. **65**, 341 (1997).
[10] N. Pizzolato, A. Fiasconaro, D. P. Adorno, and B. Spagnolo, J. Chem. Phys. **138**, 054902 (2013).
[11] B. Spagnolo and R. N. Mantegna, Nuovo Cimento D **17**, 873 (1995).
[12] A. A. Dubkov and B. Spagnolo, Phys. Rev. E **72**, 041104 (2005).
[13] A. Fiasconaro and B. Spagnolo, Phys. Rev. E **83**, 041122 (2011).
[14] Y. Hasegawa and M. Arita, J. R. Soc. Interface **9**, 3554 (2012).
[15] S. H. Kim, A. S. Panwar, S. Kumar, K. H. Ahn, and S. J. Lee, J. Chem. Phys. **121**, 9116 (2004).
[16] L. Gammaitoni, F. Marchesoni, M. Martinelli, L. Pardi, and S. Santucci, Phys. Lett. A **158**, 449 (1991).